Science of the Total Environment 622–623 (2018) 770–782

Contents lists available at ScienceDirect

Science of the Total Environment

journal homepage: www.elsevier.com/locate/scitotenv

Spatiotemporal variations of hydrogeochemistry and its controlling factors in the Gandaki River Basin, Central Himalaya Nepal

Ramesh Raj Pant [a,b,c,d,e], Fan Zhang [a,b,c,d,*], Faizan Ur Rehman [a,b,c,d,f], Guanxing Wang [a,b,c,d], Ming Ye [g], Chen Zeng [a,b], Handuo Tang [a,b,c,d]

[a] Key Laboratory of Tibetan Environment Changes and Land Surface Processes, Institute of Tibetan Plateau Research, Chinese Academy of Sciences, Beijing, China
[b] Key Laboratory of Alpine Ecology and Biodiversity, Institute of Tibetan Plateau Research, Chinese Academy of Sciences, Beijing, China
[c] CAS Center for Excellence in Tibetan Plateau Earth Sciences, Beijing, China
[d] University of Chinese Academy of Sciences, Beijing, China
[e] Central Department of Environmental Science, Tribhuvan University, Nepal
[f] Department of Earth Sciences, COMSATS Institute of Information Technology, Abbottabad, Pakistan
[g] Department of Earth, Ocean, and Atmospheric Science, Florida State University, Tallahassee, FL, USA

HIGHLIGHTS

- Strong spatiotemporal variation of geochemistry is observed in the Gandaki River.
- Hydrogeochemistry is controlled by climatic, geogenic and anthropogenic factors.
- Water facies are prevailed with Ca-HCO_3 (83%), Ca-Mg-Cl (13%) and Ca-Cl (4%).
- Water quality at a few locations poses safety concern for drinking and irrigation.

GRAPHICAL ABSTRACT

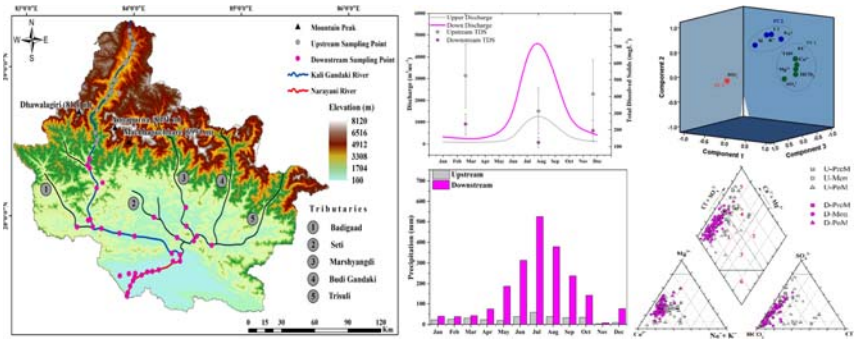

ARTICLE INFO

Article history:
Received 7 September 2017
Received in revised form 5 December 2017
Accepted 5 December 2017
Available online xxxx

Editor: G. Ashantha Goonetilleke

Keywords:
Major ions
Spatiotemporal variations
Controlling factors
Chemical weathering
Himalayan River Basin

ABSTRACT

The characterization and assessment of water quality in the head water region of Himalaya is necessary, given the immense importance of this region in sustaining livelihoods of people and maintaining ecological balance. A total of 165 water samples were collected from 55 sites during pre-monsoon, monsoon and post-monsoon seasons in 2016 from the Gandaki River Basin of the Central Himalaya, Nepal. The pH, EC values and TDS concentrations were measured in-situ and the concentrations of major ions (Ca^{2+}, Mg^{2+}, K^+, Na^+, Cl^-, SO_4^{2-}, NO_3^-) and Si were analyzed in laboratory. Correlation matrices, paired *t*-test, cluster analysis, principal component analysis (PCA), the Piper, Gibbs, and Mixing plots, and saturation index were applied to the measurements for evaluating spatiotemporal variation of the major ions. The results reveal mildly alkaline pH values and the following pattern of average ionic dominance: $Ca^{2+} > Mg^{2+} > Na^+ > K^+$ for cations and $HCO_3^- > SO_4^{2-} > Cl^- > NO_3^-$ for anions. The results of PCA, Gibbs plot and the ionic relationships displayed the predominance of geogenic weathering processes in areas with carbonate dominant lithology. This conclusion is supported by geochemically different water facies identified in the Piper plot as Ca-HCO_3 (83.03%), mixed Ca-Mg-Cl (12.73.0%) and Ca-Cl (4.24%). Pronounced spatiotemporal heterogeneity demonstrates the influence of climatic, geogenic and anthropogenic conditions. For instance, the Ca^{2+}-SO_4^{2-}, Mg^{2+}-SO_4^{2-} and Na^+-Cl^- pairs exhibit strong positive correlation with each

* Corresponding author at: Key Laboratory of Tibetan Environment Changes and Land Surface Processes, Institute of Tibetan Plateau Research, Chinese Academy of Sciences, Beijing, China.
E-mail address: zhangfan@itpcas.ac.cn (F. Zhang).

https://doi.org/10.1016/j.scitotenv.2017.12.063
0048-9697/

other in the upstream region, whereas relatively weak correlation in the downstream region, likely indicating the influence of evapo-crystallization processes in the upstream region. Analyses of the suitability of the water supply for drinking and irrigation reveal that the river has mostly retained its natural water quality but poses safety concern at a few locations. Knowledge obtained through this study can contribute to the sustainable management of water quality in the climatically and lithologically distinct segments of the Himalayan river basins.

1. Introduction

The quality of surface water, influenced by various natural and anthropogenic factors, is one of the most sensitive issues worldwide (Diamantini et al., 2018; López-Moreno et al., 2011; Singh et al., 2014; Sun et al., 2010). The chemistry of natural surface water is controlled primarily by atmospheric precipitation, chemical weathering and evapo-crystallization processes (Gibbs, 1970; Jiang et al., 2015), and secondarily by tributaries, ground water discharge, and anthropogenic interferences (Thomas et al., 2015). The study of geochemical properties of surface water has broad implications for securing water quality, as it provides an insight to understand the chemical composition and characteristics and recommend appropriate conservation measures (Şener et al., 2017; Vrebos et al., 2017). The Himalayan Rivers draining from the alpine segments of semiarid/arid region require a special understanding in terms of ionic concentrations, sediment loads, and the relevant geochemical processes (Lioubimtseva and Henebry, 2009; Xiao et al., 2012). The quality and quantity of the surface water fed by high altitude glaciers are affected by various natural and anthropogenic activities and particularly by the impacts of global climate change, across the Himalaya and Tibetan Plateau. These changes may have serious implications on livelihoods and ecosystems at local and regional levels, and thus, water and environmental sustainability requires thoughtful attention (Barnett et al., 2005; Yao et al., 2012; Zhang et al., 2012).

Catchment characteristics, such as climate, geology, land use etc., have profound impacts on hydrochemistry and water availability for human beings. For instance, the primary source of riverine Ca^{2+}, Mg^{2+}, and HCO_3^- in the hydrosphere is from the geospheric minerals with the interactions of atmospheric CO_2, whereas Na^+, Cl^-, NO_3^-, and SO_4^{2-} have multiple sources from geosphere, atmosphere, biosphere and anthroposphere (Haidary et al., 2013; Huang et al., 2009). Considering the key role of hydrochemical attributes in river water quality for the economic and ecological stability, the chemical signatures and the factors controlling the hydrochemistry of the world's major rivers have been well documented in the past decade, particularly the Amazon River (Stallard and Edmond, 1983), Ganges-Brahmaputra River (Sarin et al., 1989), Yellow River (Zhang et al., 1995), Nile River (Dekov et al., 1997), Indus River (Ahmad et al., 1998), Mississippi River (Sharif et al., 2008), Mekong River (Huang et al., 2009), Tigris River (Varol et al., 2013) and Yangtze River (Huang et al., 2009; Jiang et al., 2015). These studies have not only addressed the various sources and controlling mechanisms of hydrogeochemistry in the large river basins but also provided a remarkable information on the rates and patterns of dissolved chemicals cycle in the continent-river-ocean system.

The Himalayan ranges extending approximately 2400 km represent a lifeline that secures the water needs of humans and ecosystems, especially in the Central Himalayan region of Nepal (Paudyal et al., 2016a). Some past studies reported on specific geochemical parameters from particular segments of these Himalayan basins, such as the Seti, Koshi, Bagmati and Gandaki Rivers and to some extent highlighted the natural and anthropogenic interferences influencing the quality of water in the Himalaya (English et al., 2000; Galy and France-Lanord, 1999; Paudyal et al., 2016a; Quade et al., 2003).

The Gandaki River Basin (GRB) contains three of the world's 14 mountains peaks with the elevation over 8000 m namely Dhaulagiri, Manaslu and Annapurna (Panthi et al., 2015) (Fig.1). The main river and its tributaries draining from these Himalayas are not only the major source of drinking water and agricultural use in Nepal but also one of the major tributaries of the Ganges River System which is used by thousands of people for various purposes, e.g., domestic use, irrigation, hydropower, industrial and even ritual practices (Paudyal et al., 2016a; Singh et al., 2014; Tripathee et al., 2016). Therefore, water quality of the GRB is a matter of great concern and it is important to understand the hydrogeochemistry and major weathering processes in the basin. Recent hydrochemical studies conducted in the GRB with limited samples suggest the urgent need of comprehensive and systematic assessment of water quality in the basin (Tripathee et al., 2016; Trower, 2009).

Thus, the present study is carried out to fill the above gap with major objective to analyze the spatiotemporal variations of hydrogeochemistry and its controlling factors from two climatically and lithologically distinct segments of the GRB in the Central Himalaya, Nepal.

2. Materials and methods

2.1. Study area

The GRB, one of the three major glacier-fed river basins in Nepal, is located in the Central Himalaya and between longitudes 82.88° to 85.81°E and latitudes 27.32° to 29.33°N (Fig. 1). The GRB has one of the largest discharges among all the river basins in Nepal (Aryal, 2011). The headwater of the river lies on the southern edge of the Tibetan Plateau and flows from Nepal to India. The elevation of the GRB ranges from about 89 m in the south to >8100 m in the north, and the basin area is about 32,104 km^2 in Nepal (Dahal et al., 2016).

The Kali Gandaki is the main tributary of the GRB, which plunges its way down through the deep gorge between two peaks above 8000 m, Dhaulagiri and Annapurna. It is then joined by its major tributaries, the Trisuli, Marsyandi, Budhi Gandaki and Seti Gandaki Rivers (Bajracharya et al., 2011). The mean air temperature and annual discharge of the GRB are 17.7 °C and 1753 $m^3\ s^{-1}$, respectively. Besides, >80% of the annual precipitation is concentrated during the monsoon season from June to September (Aryal, 2011; Panthi et al., 2015).

The GRB is characterized by complex lithology, and substantial climatic and ecological variations, and a sharp contrast exists in between upstream and downstream segments along the elevation gradient (Panthi et al., 2015).The upstream segment (leeward side) of the river basin is located in the Trans-Himalayan zone between the Tibetan Plateau and the High Himalayas and experiences semi-arid climatic conditions with markedly low annual precipitation (mean ~163 mm) whereas the downstream region lies on the windward side of the Himalayas and experiences a humid, sub-tropical to temperate climate with high annual precipitation (mean ~2667 mm) (Manandhar et al., 2012; Panthi et al., 2015). The temperature and discharge also vary greatly in space and time in both segments of the basin. For instance, the minimum recorded air temperature in the upstream segment is −25 °C, while the maximum air temperature in the downstream segment reaches up to 35 °C (Paudel and Andersen, 2011; Tripathee et al., 2014). The distinct mean monthly precipitation and discharge together with the TDS concentrations obtained in this study in the two contrasting segments of the basin are shown in Fig. 1b–c.

From north to south, the Gandaki River and its tributaries drain through four major litho-tectonic units (Fig. A1) (Amatya and Jnawali,

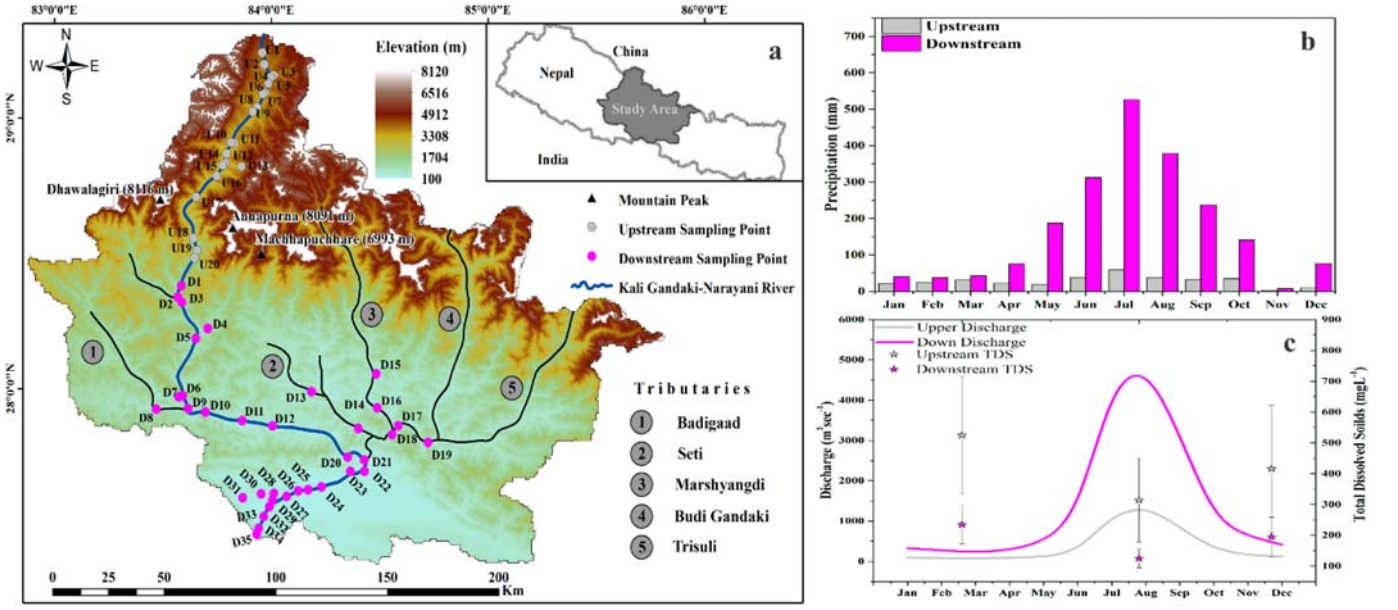

Fig. 1. a) Location map showing the sampling points in GRB, b) Mean monthly precipitation and c) Mean monthly discharge and mean TDS values in upstream (U) and downstream (D) segments of GRB. Data source: Department of Hydrology and Meteorology (DHM) of Nepal for precipitation and discharge during 2005 to 2015, and field investigations in this study for TDS during three seasons. The bars associated with the TDS values represent standard deviations.

1994): Tethyan Sedimentary Series (TSS), High Himalayan Crystalline Series (HHCS), Lesser Himalayan Crystalline Series (LHCS), and Siwalik (SW) (Dhital, 2015). In the present study, the upstream region geologically falls under the TSS and HHCS Zones, whereas the downstream is in the LHCS and SW Zones. Geologically, the TSS consists predominantly of Paleozoic and Mesozoic sedimentary rocks (e.g., limestones, shales and sandstones) with abundant fossils (e.g., cretaceous) and evaporites (e.g., halite, polyhalite, anhydrite, and gypsum) (Turchyn et al., 2013). The HHCS is dominated by metamorphic rocks: ortho-and paragneisses, migmatites, schist and calc-gneisses of Precambrian age (Galy et al., 1999; Neupane et al., 2017). The LHCS is the major geological unit comprising of green schist-grade to lower amphibolite-grade of metasedimentary rocks ranging in age from Proterozoic to Cenozoic. The SW unit is dominantly composed of mudstones, siltstones, and sandstones. Moreover, the Tarai segment is a part of Indo-Gangetic Plain (IGP) that contains alluvial sediments (Baral et al., 2017; Le Fort, 1975; Upreti, 1999).

The upstream segment of the river is mostly covered by snow/glacier with semi-arid barren land in the Higher and Trans -Himalayas whereas in the downstream, the forest and cultivable land are the major land use features. Thus, the land use/cover patterns differ between the two segments. For instance, the upstream segment features snow/glacier > grassland > barren area > forest > agriculture > shrub land > water bodies, whereas the downstream segment features forest > agriculture > grassland > shrub land > barren land > water bodies > settlements (Fig. A2) (Uddin et al., 2015).

2.2. Sampling design and analysis methods

Considering the potential impact factors such as climatic and lithological conditions, sampling campaigns were conducted in three seasons i.e., pre-monsoon (April), monsoon (August) and post-monsoon (November) in 2016. A total of 165 water samples were collected from 55 sampling sites in upstream and downstream segments of the river basin. The selection of sampling locations is based on geology, land use changes, and hydro-climatic variations with respect to elevation, topography and confluence of the major tributaries. In the upstream region, 15 and 5 number of samples were collected from the main stream and the tributaries in each sampling season, respectively. Similarly, 21 and 14 number of samples were collected from the main stream and the tributaries in each sampling season from the downstream portion of the basin, respectively. The upstream and downstream samples are indicated by the suffixes 'U' and 'D', respectively (Fig. 1, and Table A1). The sampling was difficult, especially, during the monsoon season because of heavy rainfall, high discharge, and landslides along some fragile parts of the mountain areas. However, to control relatively consistent conditions, samples were taken on the days without rainfall in 24 h.

Prior to the sample collection, each sample bottle has been washed with nitric acid for cations and then rinsed with the distilled water. In addition, the sample bottles were rinsed twice with the same river water before the sample collection. The samples were collected from approximately 20–25 cm below the surface using wide mouth high-density polyethylene (HDPE) bottles of 1000 mL which were rinsed with river water twice before the actual sampling. The pH, electrical conductivity (EC) and total dissolved solids (TDS) were measured in-situ using a multi-parameter device (HI-98129, HANNA, Romania). After that, all samples were filtered using 0.45 μm mill pore nitrocellulose filter to separate the suspended sediment and finally the filtered samples were filled in 20 mL HDPE bottles. The samples for cation analysis were preserved by acidification with 2 M HNO_3. The collected water samples were taken to the Institute of Tibetan Plateau Research, Chinese Academy of Sciences (ITP-CAS), Beijing for chemical analysis. The major cations (Ca^{2+}, Mg^{2+}, K^{+}, Na^{+}) and Si were determined using a Inductively Coupled Plasma Optical Emission Spectrometer (ICP-OES, Prodigy) with the detection limit of 0.05 ppm for Ca^{2+}, Mg^{2+}, K^{+}, and Na^{+}, and of 0.01 ppm for Si. The anions (Cl^{-}, NO_3^{-} and SO_4^{2-}) were analyzed by Ion Chromatography of Dionex ICS 900, USA with the detection limit of 0.1 ppm. Bicarbonates were determined by charge balance as described by Trower (2009).

For quality control, special care was taken during sampling and laboratory analyses. To avoid contamination, non-powder vinyl clean room gloves and masks were used during sample collection and laboratory work. The collected samples were stored in refrigerator at 4 °C until the laboratory analyses were performed i.e., about 30 days of sample collection. During the laboratory analyses, distilled deionized water was used. In addition, freshly prepared standards of known concentrations and procedural blanks were analyzed during each analytical run and no detectable contaminations were found. Furthermore, each calibration curve was evaluated by analyses of a set of samples. The average

analytical precision for both cations and anions was better than 2%. The sum of total cations (Tz^+) and anions (Tz^-) show a good match with the TDS values measured using the probe ($Tz^+ + Tz^- = 1.01TDS$, $R^2 = 0.99$), suggesting that the data are of high quality (Paudyal et al., 2016b).

The dataset obtained through field investigations and laboratory measurements, the present study includes EC, TDS, the major ions and dissolved silica data of 165 water samples from 55 sites in three seasons (Table A2). Paired *t*-tests were performed to compare the variables at different seasons for temporal variations analysis (Gotway et al., 1994). Descriptive statistics were performed to evaluate and interpret the temporal and spatial variations of the dataset. The relationship between the considered variables were examined by using correlation analysis. The data do not obey Gaussian distributions, so that the Spearman's rho correlation analysis was applied using SPSS (version 22.0) (Bishara and Hittner, 2012). Hierarchical cluster analysis (CA) based on Ward's method with Euclidean distances was applied with the intent of grouping both the sampling sites and seasons (Pacheco Castro et al., 2017; Varol et al., 2013). Principal component analysis (PCA) was applied to identify the sources of the major ions. The validity and effectiveness of PCA in reducing the dimensionality of the dataset was tested using the Kaiser-Meyer-Olkin (KMO) and Bartlett's sphericity methods (Bengraïne and Marhaba, 2003; Singh et al., 2004).

In addition, the Piper (1944), Gibbs (1970) and mixing plots were used for the further elaboration of the findings. The saturation index (SI) was calculated using the Visual MINTEQ with a built in thermodynamic database (Gustafsson, 2011), and all the graphs were made by using OrignPro version 9.3. In the end, the suitability of river water for irrigation was evaluated by estimating the Na^+% and sodium adsorption ratio (SAR), whereas drinking quality was assessed by comparing with selected major rivers around the world as well as World Health Organization (WHO) standard values.

3. Results and discussion

3.1. General hydrogeochemistry

The ionic composition of the GRB and its comparison with surrounding rivers as well as other rivers around the world are presented in Table 1. In comparison to the global average of 120 mg L^{-1} (Gaillardet et al., 1999), the GRB showed relatively higher TDS value (269 ± 172 mg L^{-1}) probably due to the semi-arid environment in the head water region of the basin. The findings of present study are supported by previous studies from the headwater region of Tibetan Plateau that showed comparable TDS values (Huang et al., 2009; Jiang et al., 2015). The pattern of cationic dominance based on mean values (mg L^{-1}) in the GRB are in the following order: $Ca^{2+} > Mg^{2+} > Na^+ > K^+$. The resutls exhibited that out of the total cationic-budget in the GRB, Ca^{2+} alone contributes 57.12%, and Ca^{2+} together with Mg^{2+} account for 77.18%. In comparison, Na^+ and K^+ account for 17.84% and 4.98%, respectively. The concentrations of Ca^{2+} and Mg^{2+} in the GRB were more than twice of the global average, which likely reflects the predominance of carbonate weathering. Relatively less intense silicate weathering was evidently shown from the average concentration of dissolved silica (3.34 mg L^{-1}) in the GRB which is slightly less than the global average (7.63 mg L^{-1}) (Meybeck, 2003). These findings are comparable to the other rivers in the region (Table 1) such as the Ganga-Brahmaputra, Upper Yangtze and Upper Mekong rivers (Huang et al., 2009; Jiang et al., 2015; Sarin et al., 1989). The results indicate that the silicate weathering is less pronounced compared to carbonate weathering in the region (Quade et al., 2003).

The average anionic concentrations (mg L^{-1}) follow a pattern of dominance that is consistent with the previous results: $HCO_3^- > SO_4^{2-} > Cl^- > NO_3^-$. The dominant anion in the GRB is HCO_3^- which accounts for 67.05% followed by SO_4^{2-} and Cl^- with 23.76% and 8.30%, respectively. The NO_3^- was reported as the least abundant anion throughout the basin with an average contribution of 0.88%. The relatively high concentrations of bicarbonates and sulphates are two and four folds of the global average, respectively, indicating the contribution of rock weathering as well as evaporite dissolutions as the main processes that determine the hydrochemistry in the basin. The anionic budget of the present study is comparable to that of other major rivers originated from the Tibetan Plateau (Huang et al., 2009; Jiang et al., 2015; Sarin et al., 1989).

3.2. Spatial variations of hydrogeochemistry

The pH was found to be neutral to alkaline for all the sampling points. The highest pH (9.16) was noted from a headwater tributary (U14) and the lowest pH (7) from the Trisuli, a downstream tributary

Table 1
Summary statistics of hydrochemical composition of the GRB and its comparison with other rivers around the world.

River		pH	EC	TDS	Ca^{2+}	Mg^{2+}	K^+	Na^+	Si	Cl^-	NO_3^-	SO_4^{2-}	HCO_3^-	Reference
Gandaki, Nepal	Mean	8.27	530	269	39.65	13.92	3.46	12.38	3.34	16.02	1.77	49.37	130.22	This study
($n = 165$)	SD	0.49	344.56	172	21.98	10.64	2.39	18.76	1.51	35.61	1.55	57.39	78.61	
	Min	7	64	34	5.92	0.39	0.73	0.74	0.61	0.33	0.20	2.28	18.78	
	Max	9.16	2006	1005	104.30	75.34	16.99	106.67	10.58	230.56	10.31	316.97	455.57	
Upstream	Mean	8.28	822	418	58.79	21.46	4.89	26.15	3.28	37.28	1.64	88.07	180.82	
($n = 60$)	SD	0.51	400.03	196.89	23.20	13.29	3.39	25.79	1.92	53.10	1.34	78.48	96	
	Min	7.20	64	34.27	5.92	0.39	1.12	0.74	0.74	0.33	0.33	2.28	18.78	
	Max	9.16	2006	1005	104.3	75.34	16.99	106.67	10.58	230.56	6.48	316.97	455.57	
Downstream	Mean	8.27	365	185	28.72	9.61	2.65	4.51	3.33	4.82	1.84	24.4	107.58	
($n = 105$)	SD	0.47	140.73	70.58	11.16	5.18	0.79	2.45	1.23	3.62	1.66	14.53	50.46	
	Min	7	111	55.87	7.16	0.92	0.73	0.88	0.61	0.42	0.20	2.88	24.4	
	Max	8.98	746	375	50.46	29	3.87	12.88	6.76	20.36	10.31	70.66	294.51	
Dudhkoshi, Nepal		7.52	37.61	37	7.90	0.40	0.70	0.80	–	0.60	1.20	3.70	22	(Paudyal et al., 2016a)
Indus, India		8.55	154	260	24	4.50	1.60	7.30	2.89	4.80	1.70	11.90	81.2	(Ahmad et al., 1998)
GB, India		8.01	—	196	28.40	11.90	2.70	14.10	4.43	6	–	14	163.70	(Sarin et al., 1989)
Pambar, India		7.15	237	151	9.67	6.77	1.88	10.54	3.33	30.66	–	4.73	71.77	(Thomas et al., 2015)
Upper Yangtze, China		7.98	—	778	53.40	22.90	5.50	157.70	—	233.70	1.30	114.90	188.50*	(Jiang et al., 2015)
Upper Mekong, China		8.42	—	302	49	14	1	12	1.86	14	–	69	138	(Huang et al., 2009)
Yellow, China		8.30	—	486	44.90	22.40	3.50	60	8.40	46.90	7.40	83.20	200.10	(Zhang et al., 1995)
Tigris, Turkey		8.45	402	276	46.61	9.14	1.44	6.43	5.92	20.70	2.49	23.20	153.80	(Varol et al., 2013)
Nile, Egypt		—	—	240	19.20	7.30	4.70	17.90	–	8.90	1.20	14.40	128.70	(Dekov et al., 1997)
Amazon, S. America		—	—	122	19.10	2.30	1.10	6.40	5.18	6.50	–	7	68	(Stallard and Edmond, 1983)
Global mean		8	—	120	15	4.10	2.30	6.30	7.63	7.80	1	11.20	58.40	(Gaillardet et al., 1999; Meybeck, 2003)
WHO limit		6–8.50	—	1000	100	50	100	200	—	250	50	250	600	(WHO, 2011)

GB: Ganga-Brahmaputra, all units in mg L^{-1}, SD: standard deviation, Min: minimum, Max: maximum, *$HCO_3^- + CO_3^{2-}$.

(D18). The upstream region is characterized by significantly higher average concentrations of EC and TDS with higher spatial variations compared to downstream region. As a result, both the highest and the lowest values of EC and TDS were recorded in the upstream region. The substantially elevated concentrations of EC and TDS in the semi-arid segment of the upstream region are most probably due to the excessive chemical weathering and physical erosion along with evaporation-crystallization processes. On the other hand, the lower concentrations of EC and TDS in downstream segment seem to be resulted from the increased precipitation and discharge (Fig. 1b–c) and the reduced impact of evaporite dissolution (Thomas et al., 2015). The TDS measured at a few sampling points (e.g., U1 and U2) in the most upstream parts containing glaciers, is found to be significantly lower compared with the whole semi-arid upstream segment (Table A1). This result is potentially due to the fact that snow and glacier meltwater dilutes the ion concentrations and alleviates the influence of evapo-crystallization processes.

Among the major cations, Ca^{2+} and K^+ display the highest and lowest concentrations, respectively, in both segments of the basin. However, the concentrations of Na^+ are much higher in the upstream than in the downstream region with large standard deviation (Table 1). Compared to the global average (Table 1), the average concentration of Na^+ was about six folds higher in the upstream whereas in downstream it is only about two folds. The concentrations of K^+ are found relatively low as compared to other cations and more or less consistent between the upstream and downstream of the river. Similarly, the average concentration of dissolved silica also displayed more or less consistent pattern in both segments of the river.

Among the major anions, HCO_3^- and NO_3^- display the highest and lowest concentrations, respectively in the upstream and downstream segments in the river basin. Relatively higher concentrations of SO_4^{2-} and Cl^- were observed in the upstream compared with the downstream region, i.e. the average values of SO_4^{2-} and Cl^- were about four and eight folds, respectively, in the upstream compared with the downstream region (Table 1). In contrast to the other major ions, the concentrations of NO_3^- show a slightly increasing trend from the upstream to the downstream (Table 1). This pattern could be explained by the dense human settlements and anthropogenic inputs in the downstream. In fact, at some of the sampling points in the downstream region, the NO_3^- concentrations are remarkably high (e.g., D9 = 10.31 mg L^{-1}), which could be due to the high anthropogenic inputs such as agriculture land use, and the Hindu's funeral sites along the bank of the river (Sharma et al., 2012).

The concentrations of most of the major ions in the downstream part of the basin were less than half of those in the upstream part of the basin, while the discharge is almost doubled in the lower part of the basin compared with the upper part. The concentrations of Na^+ and Cl^- are much higher in the upstream than the downstream due to the climatic and geological factors as the upstream area is controlled by rain shadow climate and lacustrine sediments. Some of the sampling points (e.g., U4), display relatively higher concentrations of Na^+ and Cl^- during the post-monsoon season, probably due to the accumulation of salts which were leached out from the hot water wells nearby (Jiang et al., 2015). The contrasting concentrations of the dissolved ions between the upstream and downstream segments of the GRB indicate how the climatic, hydrological and lithological differences can affect the hydrogeochemical processes in the river water.

3.3. Seasonal variations of hydrogeochemistry

The pH values are found to be alkaline during all of the sampling seasons, with slightly lower values during the monsoon period. The EC and TDS values are comparatively higher in pre-monsoon and post-monsoon than the monsoon (Pre-monsoon > Post-monsoon > Monsoon), which is one of the important characteristics of the river basins having contrast geo-environmental settings (Lewis Jr et al., 1987). The considerable variability of TDS is shown by the high standard deviations i.e. 525 ± 190 mg L^{-1}, 314 ± 136 mg L^{-1}, and 416 ± 206 mg L^{-1} during the pre-monsoon, monsoon and post monsoon, respectively in the upstream, and 234 ± 62 mg L^{-1}, 125 ± 30 mg L^{-1}, and 195 ± 64 mg L^{-1} during the pre-monsoon, monsoon and post-monsoon seasons, respectively in the downstream. These seasonal differences in TDS concentrations and their decreasing trend with increasing precipitation and discharge are shown in Fig. 1b–c.

During the pre- and post-monsoon seasons, the cationic abundance (mg L^{-1}) of the upstream water samples follows the order of $Ca^{2+} > Na^+ > Mg^{2+} > K^+$ whereas during the monsoon season, the order change to: $Ca^{2+} > Mg^{2+} > Na^+ > K^+$ (i.e., magnesium instead of sodium is the second most abundant species). However, the abundance of anions (mg L^{-1}) of the upstream water samples follows the same order of $HCO_3^- > SO_4^{2-} > Cl^- > NO_3^-$ during all the three monitoring seasons. The basin is geologically carbonate dominated so that the concentrations of bicarbonate is much higher than the other anions, resulting in consistent abundance order of anions in the upstream and downstream segments. This pattern could also be due to the effect of meltwater from the carbonate dominated lithology, which increases during the monsoon period (June to September) due to high solar radiation (Singh et al., 2014). In the downstream segment the cationic and anionic abundance follow the same order of $Ca^{2+} > Mg^{2+} > Na^+ > K^+$ and $HCO_3^- > SO_4^{2-} > Cl^- > NO_3^-$ in all the monitoring periods.

Concentrations of most major ions follow the same decreasing trend from pre-monsoon to monsoon and the same increasing from monsoon to post-monsoon (Fig. 2). The temporal variations are mainly caused by climatic conditions operating in the basin and the resulting hydrological processes. The coupled effects of high precipitation and intense melting of glaciers result in high discharge (Fig. 1b–c) which is responsible for the low concentrations of dissolved components in both segments of the river basin during the monsoon period. However, as mentioned above, unlike other major ions, the concentrations of NO_3^- shows a consistently increasing trend from pre-monsoon through monsoon to post-monsoon which may indicate the accumulated impacts of anthropogenic activities. The higher concentrations of NO_3^- in the monsoon season may be attributed to runoff from the agricultural lands with addition of nitrogenous fertilizers, and the higher concentrations in the post-monsoon season may be ascribed to the dumping of agrarian residues after major crops harvesting (Li et al., 2009b; Sharma et al., 2012). In recent years, the usage of fertilizers has increased dramatically in Nepal, as indicated by the total chemical fertilizer consumption of 12,810, 10,329, 110,013 and 144,813 metric tons in the year 2008/2009, 2009/2010, 2010/2011, 2011/2012, respectively (MOAD, 2012).

The results of the paired *t*-test comparing each sampling point with itself at different seasons are given in Table A3. All the variables exhibit significant differences ($p < 0.05$) in all the seasons only with exception of pH, K^+ and HCO_3^- between pre-and post-monsoon seasons. It is shown that most chemical attributes have highest values in pre-monsoon season but lowest values in the monsoon season under the impact of monsoon driven precipitation and river discharge seasonality.

3.4. Characterization of hydrogeochemical facies

The milli-equivalent percentage (meq%) of major ions are plotted in Piper (1944) diagram and further projected into central diamond field to evaluate the hydrogeochemical facies and types of water (Fig. 3 and Table A4). On the cation plot, most of the samples lies in the lower left corner, indicating the dominance of calcium in the river water (Fig. 3). In addition, a few samples from the downstream region especially those from some tributaries show relatively higher concentrations of Mg^{2+} (i.e. D16, D20 and D31). Some of the water samples from the upstream region display increased concentrations of sodium and potassium ions, which indicate the influence of local sources of Na^+ and K^+ (Karim and Veizer, 2000). However, the overall characteristics are still consistent with carbonate-dominated lithology. The anion diagram

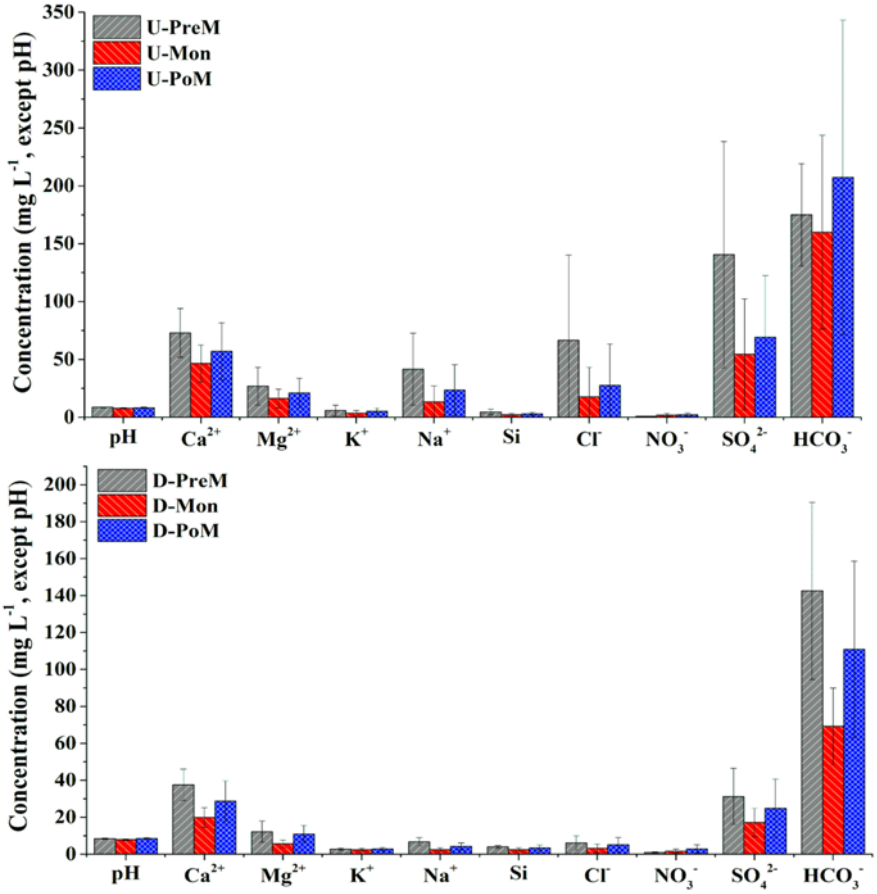

Fig. 2. Seasonal variation of hydrogeochemistry in upstream (U) and downstream (D) segments of GRB in pre-monsoon (PreM), monsoon (Mon) and post-monsoon (PoM). The bars associated with the ionic values represent the standard deviations.

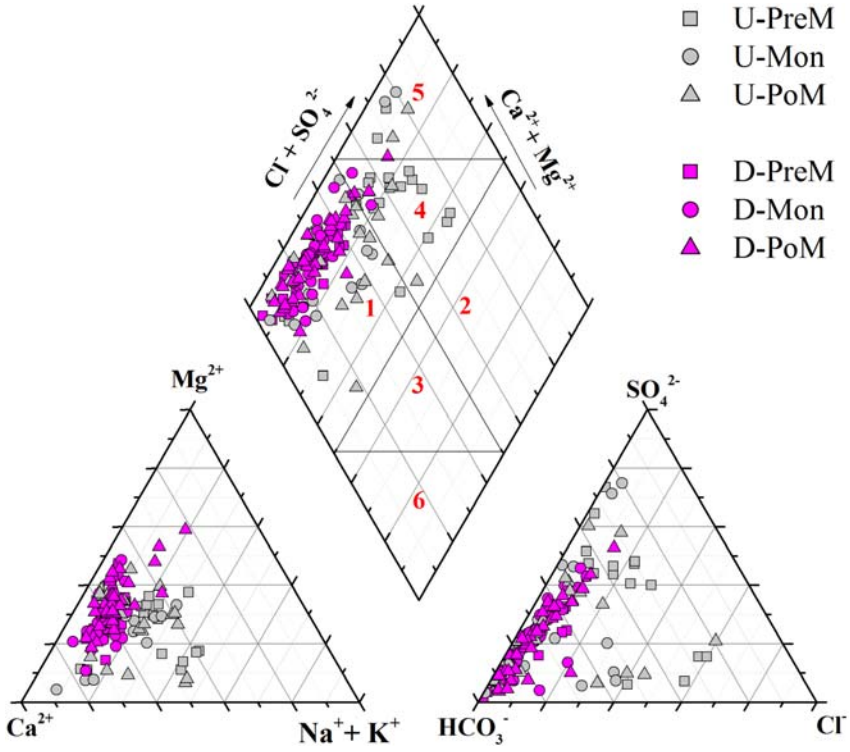

Fig. 3. Piper diagram characterizing the hydrochemistry in upstream (U) and downstream (D) segments of GRB during pre-monsoon (PreM), monsoon (Mon) and post monsoon (PoM) seasons.

shows that most of the water samples fall on lower left corner near the HCO_3^- apex (Fig. 3), again signifying the carbonate dominated lithology. Nevertheless, majority of the water samples in all the sampling seasons from the upstream region were more enriched with Cl^- and SO_4^{2-} compared to the downstream samples, demonstrating the influence of evaporites though the concentrations were relatively less pronounced during monsoon season.

The results plotted in the central diamond field show the overall characteristics of river water chemistry: the dominance of the alkaline earth elements (Ca^{2+} and Mg^{2+}) over the alkalines (Na^+ and K^+) and the weak acids (HCO_3^-) over the strong acids (Cl^- and SO_4^{2-}). Generally, six sub-fields can be identified in the diamond Piper diagram: 1) Ca-HCO_3, 2) Na-Cl, 3) Mixed Ca-Na-HCO_3, 4) Mixed Ca-Mg-Cl, 5) Ca-Cl, and 6) Na-HCO_3 (Khadka and Ramanathan, 2012). The hydrogeochemical results shown in this study are confined only into three types as representing the carbonate dominant lithology, for example, 83.03% of the water samples belong to the Ca-HCO_3 type, 12.73% belong to the Ca-Mg-Cl type (mostly from the upstream during pre-monsoon), and 4.24% belong to the Ca-Cl type (Table A4). Six out of seven samples representing the Ca-Cl type of water are from the upstream region and only one sample is from a tributary of the downstream region (D15). The higher concentrations of Cl^- in the downstream samples may be attributed to solid and liquid wastes from nearby settlements, cremation sites and religious places for holy bath etc. (Bhatnagar et al., 2016; Sharma et al., 2012).

In general, no significant change was observed in the hydrogeochemical facies in the river water samples over the entire monitoring period, which clearly indicates that most of the major ions are of natural origin. However, spatial heterogeneity is visible as the upstream water showed both carbonate and evaporite dominated features (Ca-HCO_3 type, Ca-Mg-Cl type and Ca-Cl type) whereas mostly carbonate dominated features (Ca-HCO_3) are found in downstream region.

3.5. Association among the hydrogeochemical attributes

3.5.1. Correlation matrix

Correlation matrix is a widely used statistical tool to establish the relationship between two hydrogeochemical variables for predicting the degree of dependency of one variable to the other (Ramanathan, 2007). The correlation matrices of this study are presented in Table A5, exhibiting the correlation among the hydrogeochemical variables in the upstream and downstream segments of the GRB. The Ca^{2+}-Mg^{2+}, Ca^{2+}-HCO_3^- and Mg^{2+}-HCO_3^- pairs show positive correlations in both river segments, implying a common origin of these ions which is most probably related to intense weathering of carbonate rocks (Singh et al., 2016). Other, strong positive correlations were observed between the Ca^{2+}-SO_4^{2-} and Mg^{2+}-SO_4^{2-} pairs in the upstream segment, evidencing the association of river water with evaporites and soil salts (epsom, gypsum/anhydrite). The strong positive correlation of Cl^- with Na^+ supports the interaction of halite with river water and indicates the local lithogenic sources of these two ions (Jiang et al., 2015). There is no significant correlation between Cl^- and SO_4^{2-} in the upstream, but in the downstream segment (Table A5), suggesting different sources of chloride and sulphate in the upstream, and similar sources in the downstream segments. Si shows strong negative correlation with SO_4^{2-} in the upstream but no significant correlation with any other ion in the downstream, indicating a different source of origin for these ions. In addition, Si shows no significant correlation with neither TDS nor HCO_3^- confirming that the silicate weathering is less intense in the basin. Finally, NO_3^- is not significantly correlated with any of the other variables, indicating potential anthropogenic interferences with the natural water quality (Li et al., 2009a).

3.5.2. Cluster analysis

The Hierarchical clustering approach has been successfully applied in hydrogeochemical studies to group similar sampling sites and/or geochemical constituents with similar characteristics, which are affected by similar processes and sources (Pacheco Castro et al., 2017; Saleh and Shehata, 1999). The cluster analysis was performed to group similar water samples in the GRB based on the major ion concentrations of three different seasons from 55 sites. Fig. 4 represents a dendrogram which groups 165 water samples into four statistically significant clusters with low distance criterion between 0 and 5 in a very convincing way. The classifications varied with significant level because each cluster is recognized by a different hydrological, geological and climatic conditions. In cluster 1, 53 out of 59 of the samples were collected from the downstream, with 39.6%, 24.5%, and 35.8% in the pre-monsoon, monsoon and post-monsoon seasons, respectively. The samples in cluster 1 reflect river water with low ionic strengths. The presence of a small number of samples from the upstream region in cluster 1 mostly indicates dilution by meltwater. In cluster 2, 35 out of 41 of the samples were collected from the downstream, with 8.6%, 62.9%, and 28.6% in the pre-monsoon, monsoon and post-monsoon seasons, respectively, indicating strong seasonality of diluted river water from downstream in monsoon season. In cluster 3, 10.0%, 55.0%, and 35.0% of the 20 upstream samples were collected in the pre-monsoon, monsoon, and post-monsoon seasons, respectively, whereas 52.9%, 5.9%, 41.2% of the 17 downstream samples were collected in the pre-monsoon, monsoon, and post-monsoon seasons, respectively. The samples in cluster 3 indicate moderately mineralized river water. In cluster 4, all the samples were collected in the upstream, with 84.6% and 15.4% in the pre- and post-monsoon seasons, respectively, reflecting highly mineralized water.

The grouping of samples illustrated by the cluster analysis results indicate the spatial variation as the primary characteristics and seasonal variation as the *sec*ondary characteristics. The findings are in good agreement with previous studies emphasizing that both spatial features and temporal aspects should be considered for the design of water monitoring networks in the contrasting segment of the river basins (Lecomte et al., 2005; Thomas et al., 2015).

3.5.3. Principal component analysis (PCA)

PCA is a powerful technique applied to the geochemical dataset to reduce the dimensionality consisting of a large number of interrelated variables (Singh et al., 2004). Based on the 165 water samples collected during the three seasons at 55 sites, PCA analysis was applied to the measurements of EC and the concentrations of TDS and the major ions including dissolved silica, to identify the variables with the greatest explanatory power that govern the chemical composition of the river water. The results of principal components (PCs), variable loadings and explained variance are presented in Fig. 5 and Table A6. It is indicated that three PCs explain 82.7% of the total variance. PC1 accounts for 47.8% and has strong loadings on EC, TDS, Ca^{2+}, Mg^{2+}, SO_4^{2-} and HCO_3^- and a moderate loading on Na^+. The colocations of these hydrochemical attributes indicate carbonate weathering as the governing source of these contents, with concurrence of evaporite dissolution. PC2 explains 25.5% of the total variance, with strong loadings on K^+, Na^+, and Cl^- and a moderate loading on Si. The colocation of the parameters indicate that mixed sources, such as atmospheric inputs, evaporite dissolution and silicate weathering may be the dominant sources of these ions. PC3 accounts for 9.4% of the total variance and has a strong loading on NO_3^-, which reflects potential contributions from anthropogenic activities (Sun et al., 2010).

3.6. Major sources and controlling factors of hydrogeochemistry

During the entire monitoring period, the mean molar ratios of Na^+ / Cl^- (>2) and K^+ / Cl^- (>0.46) in the two segments of the river basin are much higher than the corresponding ratios in marine water (Na^+ / Cl^- = 0.86 and K^+ / Cl^- = 0.02). This fact indicates that the contribution of atmospheric inputs is very low in both spatial and temporal scales in the GRB (Singh et al., 2014; Xiao et al., 2012). Given that the Na^+/Cl^- ratio is

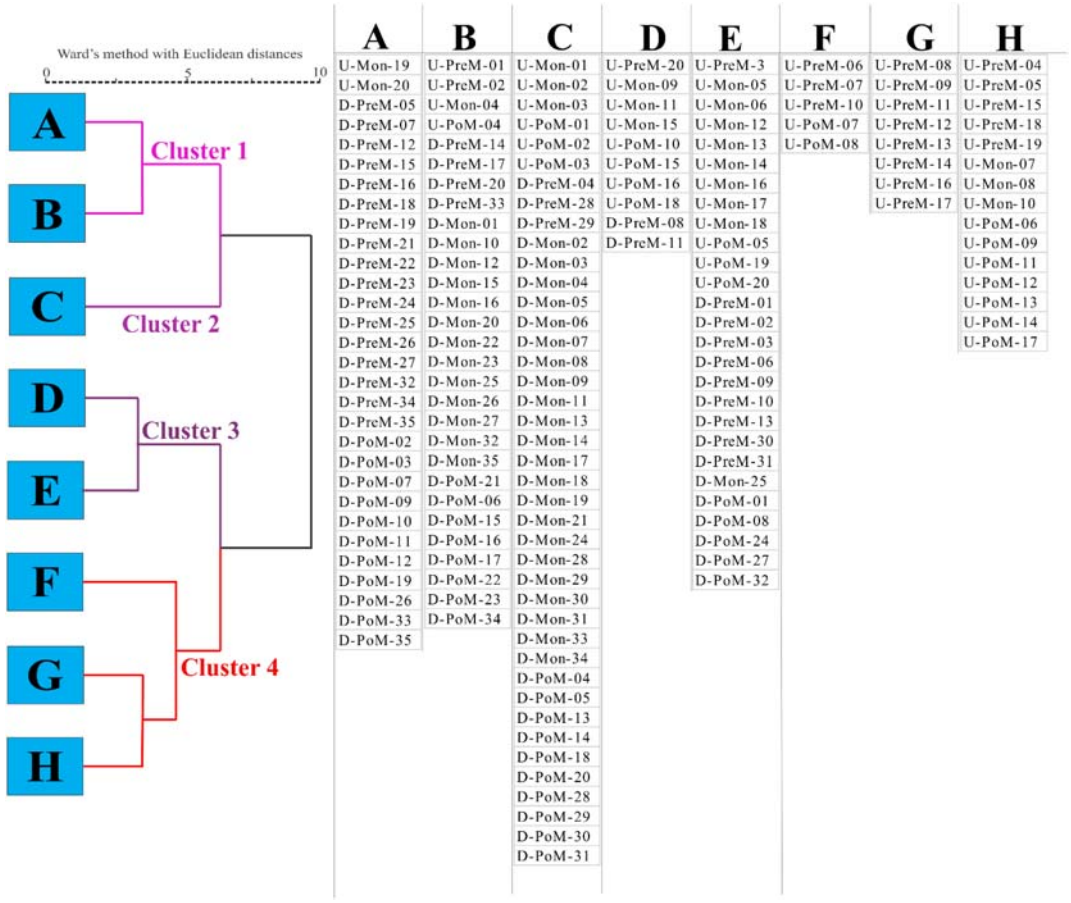

A	B	C	D	E	F	G	H
U-Mon-19	U-PreM-01	U-Mon-01	U-PreM-20	U-PreM-3	U-PreM-06	U-PreM-08	U-PreM-04
U-Mon-20	U-PreM-02	U-Mon-02	U-Mon-09	U-Mon-05	U-PreM-07	U-PreM-09	U-PreM-05
D-PreM-05	U-Mon-04	U-Mon-03	U-Mon-11	U-Mon-06	U-PreM-10	U-PreM-11	U-PreM-15
D-PreM-07	U-PoM-04	U-PoM-01	U-Mon-15	U-Mon-12	U-PoM-07	U-PreM-12	U-PreM-18
D-PreM-12	D-PreM-14	U-PoM-02	U-PoM-10	U-Mon-13	U-PoM-08	U-PreM-13	U-PreM-19
D-PreM-15	D-PreM-17	U-PoM-03	U-PoM-15	U-Mon-14		U-PreM-14	U-Mon-07
D-PreM-16	D-PreM-20	D-PreM-04	U-PoM-16	U-Mon-16		U-PreM-16	U-Mon-08
D-PreM-18	D-PreM-33	D-PreM-28	U-PoM-18	U-Mon-17		U-PreM-17	U-Mon-10
D-PreM-19	D-Mon-01	D-PreM-29	D-PreM-08	U-Mon-18			U-PoM-06
D-PreM-21	D-Mon-10	D-Mon-02	D-PreM-11	U-PoM-05			U-PoM-09
D-PreM-22	D-Mon-12	D-Mon-03		U-PoM-19			U-PoM-11
D-PreM-23	D-Mon-15	D-Mon-04		U-PoM-20			U-PoM-12
D-PreM-24	D-Mon-16	D-Mon-05		D-PreM-01			U-PoM-13
D-PreM-25	D-Mon-20	D-Mon-06		D-PreM-02			U-PoM-14
D-PreM-26	D-Mon-22	D-Mon-07		D-PreM-03			U-PoM-17
D-PreM-27	D-Mon-23	D-Mon-08		D-PreM-06			
D-PreM-32	D-Mon-25	D-Mon-09		D-PreM-09			
D-PreM-34	D-Mon-26	D-Mon-11		D-PreM-10			
D-PreM-35	D-Mon-27	D-Mon-13		D-PreM-13			
D-PoM-02	D-Mon-32	D-Mon-14		D-PreM-30			
D-PoM-03	D-Mon-35	D-Mon-17		D-PreM-31			
D-PoM-07	D-PoM-21	D-Mon-18		D-Mon-25			
D-PoM-09	D-PoM-06	D-Mon-19		D-PoM-01			
D-PoM-10	D-PoM-15	D-Mon-21		D-PoM-08			
D-PoM-11	D-PoM-16	D-Mon-24		D-PoM-24			
D-PoM-12	D-PoM-17	D-Mon-28		D-PoM-27			
D-PoM-19	D-PoM-22	D-Mon-29		D-PoM-32			
D-PoM-26	D-PoM-23	D-Mon-30					
D-PoM-33	D-PoM-34	D-Mon-31					
D-PoM-35		D-Mon-33					
		D-Mon-34					
		D-PoM-04					
		D-PoM-05					
		D-PoM-13					
		D-PoM-14					
		D-PoM-18					
		D-PoM-20					
		D-PoM-28					
		D-PoM-29					
		D-PoM-30					
		D-PoM-31					

Fig. 4. Dendrogram showing the clustering of water samples from 55 sites in upstream (U) and downstream (D) segments of GRB during pre-monsoon (PreM), monsoon (Mon) and post monsoon (PoM) seasons.

larger than 1 (Table 2) and silicate weathering is less intense, the Na^+ is believed to be released mainly from Na-bearing salts (Meybeck, 1987). Moreover, the contribution of atmospheric inputs is expected to decrease with increasing distance from the sea (Stallard and Edmond, 1983). The increase of the ratios from the downstream to the upstream is most likely due to local sources, such as evaporates dissolution, rather

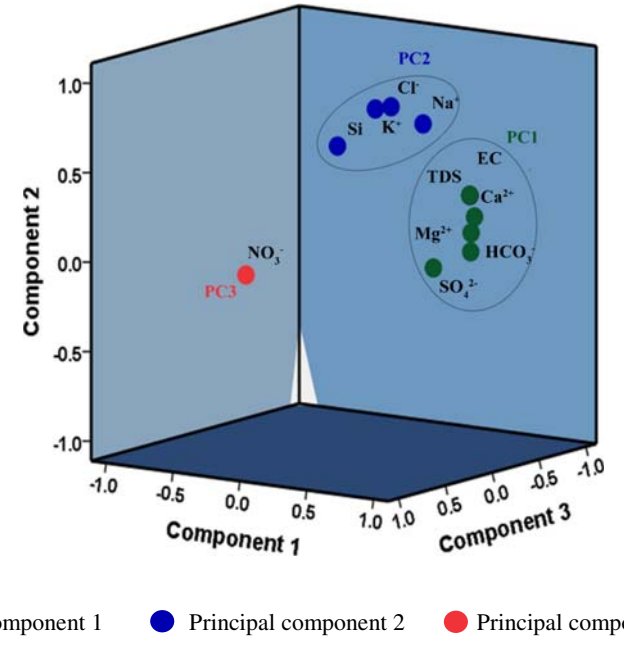

Fig. 5. Factor loading plot of the principal component analysis for EC, TDS, major ions and dissolved silica in GRB.

Table 2
Ionic ratios of various hydrogeochemical attributes (used for this study) from upstream (U) and downstream (D) segments of GRB during pre-monsoon (PreM), monsoon (Mon) and post monsoon (PoM) seasons.

Parameter	Upstream			Downstream			Grand mean
	PreM	Mon	PoM	PreM	Mon	PoM	
Ca^{2+} / Na^{+}	3.26 (0.96–9.73)	8.33 (1.38–16.11)	5.15 (1.16–13.65)	6.94 (3.98–15.29)	10.36 (4.55–26.31)	8.70 (1.62–17.02)	6.77
Mg^{2+} / Na^{+}	1.74 (0.28–6.42)	4.53 (0.66–11.78)	2.64 (0.20–8.44)	3.69 (1.07–10.48)	5.09 (0.96–18.36)	5.46 (2.03–14.07)	3.69
HCO_3^- / Na^{+}	2.66 (0.58–8.43)	8.52 (2.28–21.73)	5.51 (1.09–20.50)	8.88 (4.04–22.47)	11.54 (3.35–29.26)	10.96 (2.54–24.14)	7.36
HCO_3^- / Ca^{2+}*	1.69 (0.80–3.46)	2.21 (0.69–3.34)	2.25 (0.53–3.44)	2.47 (1.92–3.97)	2.32 (1.30–3.37)	2.62 (1.03–7.87)	2.15
HCO_3^- / (Na^{+} + K^{+})	2.40 (0.54–7.18)	6.32 (2.00–15.60)	4.49 (0.98– 18.78)	7.08 (3.43–17.54)	6.99 (2.47–14.46)	7.58 (2.04–15.91)	5.20
(Ca^{2+} + Mg^{2+}) / (Na^{+} + K^{+})*	4.57 (1.27–14.77)	9.56 (2.40–19.39)	6.16 (1.21–20.07)	8.50 (4.57–18.82)	9.23 (4.25–20.67)	9.79 (3.34–20.11)	7.46
Ca^{2+} / SO_4^{2-}	3.14 (0.76–11.37)	4.56 (0.76–26.35)	3.28 (0.65–9.56)	4.28 (1.71–27.58)	3.48 (1.46–11.13)	4.11 (0.85–15.97)	3.60
Na^{+} / Cl^{-}	2.26 (0.67–7.52)	2.72 (0.25–13.33)	2.74 (0.89–9.21)	2.26 (1.06–6.37)	1.78 (0.16–6.66)	2.32 (0.29–13.95)	2.28
Si / (Na^{+} + K^{+})	0.32 (0.03–1.94)	0.45 (0.07–1.50)	0.35 (0.04–1.30)	0.85 (0.33–2.52)	1.10 (0.32–2.77)	1.01 (0.17–3.58)	0.65
HCO_3^- / (HCO_3^- + SO_4^{2-})	0.56 (0.23–0.93)	0.71 (0.20–0.96)	0.69 (0.33–0.94)	0.77 (0.63–0.98)	0.76 (0.49–0.94)	0.76 (0.37–0.96)	0.68
(Ca^{2+} + Mg^{2+}) / Tz^{+}	0.76 (0.56–0.93)	0.86 (0.70–0.95)	0.79 (0.54–0.95)	0.88 (0.82–0.95)	0.89 (0.81–0.95)	0.89 (0.77–0.95)	0.83
(Na^{+} + K^{+}) / Tz^{+}	0.23 (0.06–0.43)	0.13 (0.04–0.45)	0.20 (0.04–0.45)	0.11 (0.05–0.17)	0.10 (0.046–0.19)	0.10 (0.04–0.23)	0.16

Values expressed as mean and range (in parenthesis), all ratios derived from μeq, * ratios from μmolar concentrations, Tz^{+}: sum of total cations in μeq.

than the contribution of sea salts. Similar results have also been reported in the Yangtze and Upper Han River Basins of China (Chen et al., 2002; Huang et al., 2008).

When identifying major sources and controlling factors of hydrogeochemistry, it is necessary to differentiate anthropogenic inputs from natural inputs in the river basin as the surface water chemistry can also be greatly affected by anthropogenic interferences (Flintrop et al., 1996). Changes in climate and land use in the headwater region of the Tibetan Plateau may introduce variations in the chemical composition of the downstream river water (Chen et al., 2002; Guo et al., 2015; Wang et al., 2007). In addition, anthropogenic influence is inferred from the relatively high contents of NO_3^- in the downstream segment of this study, where the use of nitrogen fertilizers in the cultivable land along the river bank may increase the nitrate concentrations in the river water. The results are also supported by the absence of correlations between NO_3^- and the other hydrogeochemical variables (Table A5).

The mechanisms controlling the hydrogeochemistry of surface water can be inferred from the three end member in Gibbs schematic diagram (Fig. 6): (1) End member 1 has low TDS (<10 mg L^{-1})

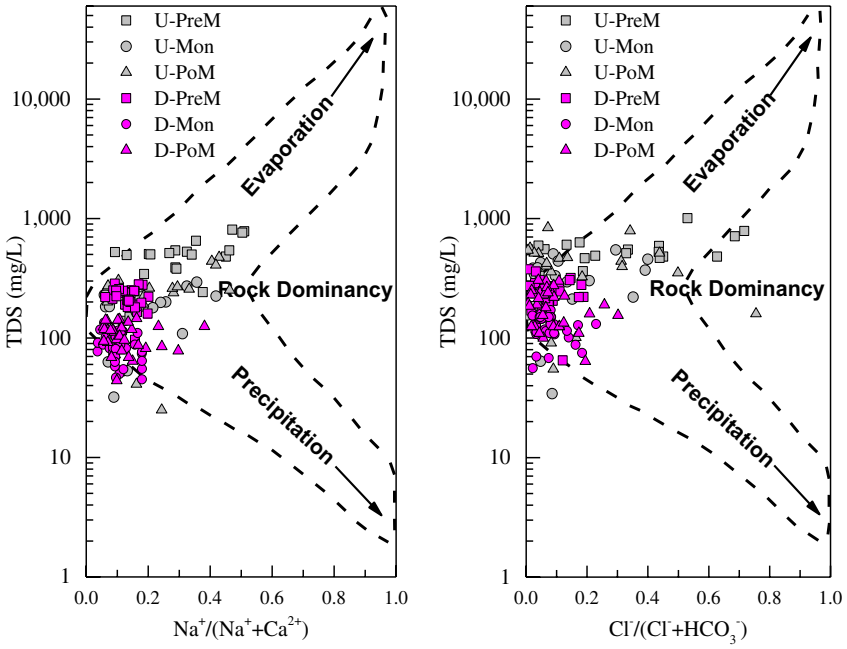

Fig. 6. Spatiotemporal variation of the weight ratio of Na^{+} / (Na^{+} + Ca^{2+}) and Cl^{-} / (Cl^{-} + HCO_3^-) as a function of TDS in Gibbs diagram (1970) from upstream (U) and downstream (D) segments of GRB during pre-monsoon (PreM), monsoon (Mon) and post monsoon (PoM) seasons.

concentrations and high ratios of $Na^+ / (Na^+ + Ca^{2+})$ and $Cl^- / (Cl^- + HCO_3^-)$ (0.5–1), and is located in the lower right corner and reflecting the influence of precipitation; (2) End member 2 has medium TDS (70 to 300 mg L^{-1}) concentrations and low ratios of $Na^+ / (Na^+ + Ca^{2+})$ and $Cl^- / (Cl^- + HCO_3^-)$ (<0.5), and is located in the left side of center and demonstrating the predominance of rock weathering; and (3) End member 3 has high TDS (>300 mg L^{-1}) concentrations and high ratios of $Na^+ / (Na^+ + Ca^{2+})$ and $Cl^- / (Cl^- + HCO_3^-)$ (0.5–1), and is located in the upper right corner and indicating the dominancy of evaporite dissolution (Gibbs, 1970; Jiang et al., 2015; Stallard and Edmond, 1987).

The locations of the samples collected in the two segments of the GRB in the Gibbs diagram (Fig. 6) illustrate the dominancy of geogenic factors in both segments of the GRB. However, most of the water samples in the upstream region were characterized by relatively higher concentrations of TDS and wide ranges of $Na^+ / (Na^+ + Ca^{2+})$ and $Cl^- / (Cl^- + HCO_3^-)$ ratios compared to the downstream segment, evidencing the major role of evaporation-crystallization processes in sedimentary geological settings as a major controlling factor of hydrogeochemistry (except for a few samples that reflect the effects of meltwater). This trend is almost constant in the upstream region for all the sampling seasons which is most likely because of the semi-arid rain shadow zone, where the influence of dilution from precipitation is relatively low. On the other hand, in the downstream region, most of the samples displayed moderate TDS and low ratios of $Na^+ / (Na^+ + Ca^{2+})$ and $Cl^- / (Cl^- + HCO_3^-)$, indicating the dominance of rock weathering. The results of Gibbs plot for this study particularly in downstream region are in good agreement with those obtained for the rivers from the Mountain Everest region and the Indus basin draining from similar lithological and climatic environment (Ahmad et al., 1998; Paudyal et al., 2016a).

3.7. Chemical weathering

The chemical weathering (calcite, dolomite, Ca-, Na- and K-feldspar) and the evaporite dissolution (halite, anhydrite and gypsum) yield different combinations of dissolved ions which play vital role in controlling the hydrogeochemistry of river water. The weathering of carbonates generates Ca^{2+}, Mg^{2+}, and HCO_3^-, weathering of silicates generates Ca^{2+}, Mg^{2+}, Na^+, K^+, Si and HCO_3^- and dissolution of evaporites generates Ca^{2+}, Mg^{2+}, Na^{2+}, K^{2+}, SO_4^{2-}, and Cl^-. In other words, Ca^{2+} and Mg^{2+} primarily originate from the weathering of carbonates, silicates and evaporites, Na^+ and K^+ from the dissolution of evaporites and the weathering of silicates and SO_4^{2-} and Cl^- from the evaporites dissolution. With respect to the anions, HCO_3^- is predominantly derived from the weathering of carbonate and silicates minerals, whereas Cl^- and SO_4^{2-} are mainly derived from the halite, sulfide oxidation and soft sulphate minerals such as gypsum (Galy and France-Lanord, 1999; Mortatti and Probst, 2003; Thomas et al., 2015). As a result, the weathering of the representative lithologies generates various combinations of ions illustrated by different ionic ratios in a solution. To identify the origins of the major ions produced by chemical weathering, the ionic ratios of water samples for pre-monsoon, monsoon and post-monsoon of the GRB are depicted in Table 2.

Previous studies suggested that ratios of HCO_3^- / Ca^{2+} close to 2 indicate the control of carbonate weathering on water chemistry (Thomas et al., 2014). In this study, the mean molar ratio of HCO_3^-/Ca^{2+} is 2.15, which confirms that carbonate weathering plays a crucial role in hydrogeochemistry of the GRB. The high mean ratios of $(Ca^{2+} + Mg^{2+}) / (Na^+ + K^+)$ (7.46) and $HCO_3^- / (Na^+ + K^+)$ (5.20) also suggest that the basin is dominated by the weathering of calcite and dolomite minerals. However, these ratios display considerable spatial differences due to the buffering of carbonate dominated hydrogeochemistry by evaporites dissolution in the upstream segment of the basin.

Generally, carbonates have higher solubility (12–40 times) than silicates and are more susceptible to weathering under natural conditions (Meybeck, 1987). In the present study, the relatively high grand mean ratio of $Ca^{2+} + Mg^{2+} / Tz^+$ (0.83) and low ratio of $Na^+ + K^+ / Tz^+$ (0.16), suggests that the silicate and evaporate weathering is less intense compared to carbonates (Table 2). This conclusion is also supported by the absence of significant correlation between Si and Na^+, K^+, Ca^{2+} and Mg^{2+} during the monitoring periods in the basin (Fan et al., 2014; Moon et al., 2009). For the chemical weathering of carbonate rocks, a proton source is required. Thus, the relative importance of two proton producing reactions i.e. carbonation and sulfide oxidation can be explained on the basis of $HCO_3^- / (HCO_3^- + SO_4^{2-})$ ratios (C-ratio). If the C-ratio is <0.50, the coupled chemical reactions of both carbonate dissolution and sulfide oxidation are indicated, whereas if the ratio is close to 1, exclusively carbonation reactions and dissociation of CO_2 deriving protons from atmospheric inputs. In the present study, the mean C-ratios of both the up- and down-stream segments of the GRB were >0.50 and grand mean ratios was 0.68, specifying the importance of carbonate and CO_2 dissolution in proton producing mechanisms. Additionally, the high ratio of Ca^{2+} / SO_4^{2-} (>3) for both segments of river during the entire monitoring periods further confirms that H_2SO_4 does not replace H_2CO_3 as a major source of protons for rock weathering in the GRB as also discussed elsewhere (Singh et al., 2014).

The spatiotemporal variability in the hydrogeochemistry of the river basin is illustrated by mixing diagrams of Na-normalized molar ratios (μeq) of Ca^{2+} versus HCO_3^- and Ca^{2+} versus Mg^{2+}. The main feature of water derived from the semi-arid/arid environments of the river basin is the depletion of HCO_3^- compared to the concentrations of Ca^{2+} and Mg^{2+} (Gaillardet et al., 1999). In the present study, most of the downstream samples are located towards the carbonate end-member indicating dominance of carbonate weathering, while some of the upstream samples are located near the evaporite and silicate end-members, indicating that the sampling points are likely located near the environments where evaporites dissolve and high silicate weathering (Fig. 7a and b).

In summary, all of these ionic relations indicate that the hydrogeochemistry of the basin is mainly regulated by carbonate weathering and evaporites dissolution followed by minor contributions from silicate weathering. However, to acquire the more reliable concentrations of HCO_3^- in the river water, it should be measured in the field, or at least before 24 h after sampling, following the standard methods (Apha, 2005).

3.8. Saturation index (SI)

The precipitation of minerals can also have considerable influence on the river water chemistry, which can be analyzed by using the saturation index (SI). The SI values indicate the saturation state of waters with respect to different minerals (SI < 0, undersaturation; SI = 0, equilibrium; and SI > 0, oversaturation) (Peter and Anandhan, 2008; Xiao et al., 2015). As shown in Fig. A3, the calculated SI values were compared with the range of 0 ± 0.50 considering the uncertainty in the saturation index equilibrium (Hiroshi et al., 1999). In most of the samples, the calculated SI values (Table A7, Fig. A3) showed the oversaturation of carbonate minerals during pre-monsoon and post-monsoon, and under saturation during monsoon in both the segments of the basin. Particularly, the river water is oversaturated with respect to, calcite and dolomite (SI > 0) and undersaturated with respect to quartz (SI < 0) in both the segments, whereas during the monsoon season the river water is primarily undersaturated.

The results confirm that the carbonate minerals have substantial control over the silicate minerals. However, the degree of influence varies spatially and temporally, which could be due to the distinctly diverse nature of lithological and climatic environments along with some anthropogenic interferences (in downstream regions).

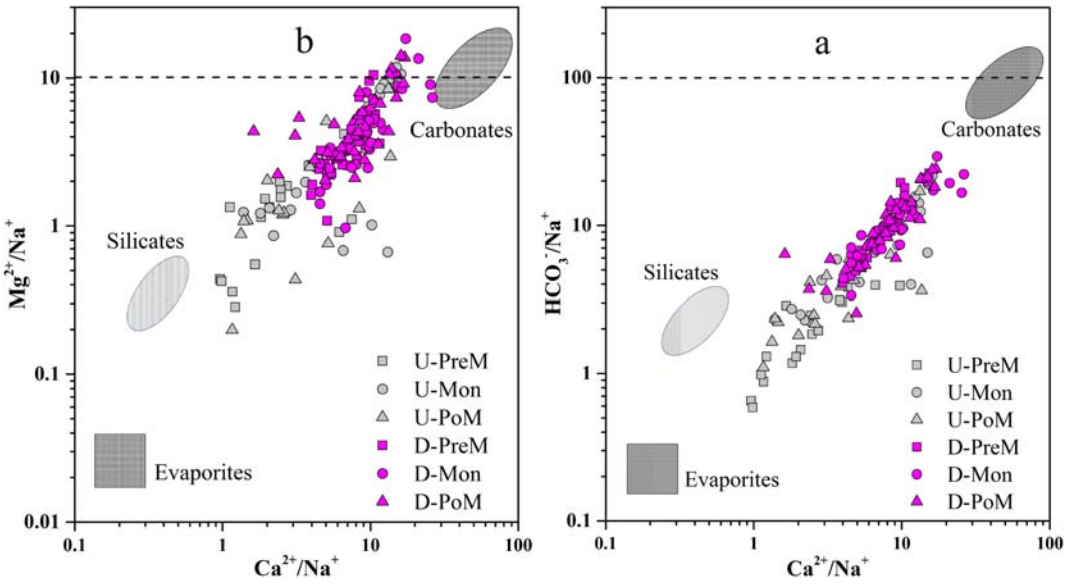

Fig. 7. Mixing diagram of Na-normalized molar ratios of (a) Ca^{2+} versus HCO_3^- and (b) Ca^{2+} versus Mg^{2+} in upstream (U) and downstream (D) segments of GRB during pre-monsoon (PreM), monsoon (Mon) and post-monsoon (PoM) seasons. The data for the three endmembers, i.e., carbonates, silicates and evaporites, are obtained from Gaillardet et al. (1999).

3.9. Suitability for drinking and irrigation quality

The river water is widely used for drinking and other domestic purposes in the basin and nearly 1.2 million people are dependent on the water from the river (Mishra et al., 2014). Therefore, the water quality is one of the important parameters directly affecting both the human and ecosystem health. Apart from this, the agriculture is one of the major income sources in Nepal (64% households and 35% of the national GDP), and it directly depends upon rain-fed and irrigational water (Dahal et al., 2016). Thus, the suitability of water for drinking and irrigation purposes has great concern for human and crop health perspective in the basin (Thomas et al., 2014). The present study shows that the river water quality is mostly within the safe limits of WHO guideline for drinking water quality in terms of ionic concentrations except for a few samples (Table A2). For instance, 1 sample (U10), 2 samples (U9 and U10), 1 sample (U10), 3 samples (U3, U6 and U10) and 2 samples (U10 and U14) exceed the maximum permissible limits for TDS, Ca^{2+}, Mg^{2+}, Na^+, and SO_4^{2-}, respectively. In addition, 2 samples (U8 and U14), 1 sample (U9) and 1 sample (U13) shows Ca^{2+}, Mg^{2+}, and SO_4^{2-} concentrations close to the limits, respectively. All of the samples with above parameters exceeding or closer the WHO guideline values were from the core semi-arid segment of the basin in the pre-and post-monsoon seasons (Table A2).

The suitability of water for irrigation depends upon type and concentrations of dissolved salts where Na^+ plays a vital role (Elango, 2005). Generally, high sodium contents in irrigation water causes the displacement of Ca^{2+} and Mg^{2+} by Na^+. The displacement of Ca^{2+} and Mg^{2+} in soil reduces its permeability which affects the crop yield causing calcium deficiency, deflocculation and impairment of the tilth. Thus, the suitability of river water for irrigation can be assessed by estimating Na^+% and sodium adsorption ratio (SAR) (Eqs. (1) and (2)) (Richards, 1954; Thomas et al., 2014);

$$Na^{+}\% = \left[\left(Na^{+} + K^{+}\right)/\left(Ca^{2+} + Mg^{2+} + Na^{+} + K^{+}\right)\right] \times 100 \quad (1)$$

$$SAR = Na^{+}/\sqrt{\left(Ca^{2+} + Mg^{2+}\right)/2} \quad (2)$$

where, concentrations are expressed in meq L^{-1}.

The irrigation water can be classified into five categories based on Na^+% values (excellent <20, good: 20–40, permissible: 40–60, doubtful: 60–80 and unsuitable >80) (Richards, 1954; Wilcox, 1948). The calculated values of Na^+% and SAR in the GRB are depicted in Table A8, and compared with standard values in Table A9. The grand mean value of Na^+% in the GRB was 14.10 ± 8.18, indicating excellent quality of water for irrigation purposes (Table A8). The Na^+% values were relatively lower during the monsoon when compared to pre-and post-monsoon seasons in both segments. Comparing to the spatial scale, relatively higher values were found in the upstream segment of the basin. The Na^+% values fell under the excellent to permissible category for the irrigation as 82.42% excellent, 13.94% good and 3.64% permissible (Table A9).

Based on the SAR values, irrigation water is classified into four groups (low <10, medium: 10–18, high: 18–26 and very high: >26)(Saleh and Shehata, 1999; Thomas et al., 2014), with high SAR values indicating increased danger to the crops. In this study (Table A8), the SAR values for all the samples are <3 during the entire monitoring period and the grand mean value is 0.37 ± 0.41 which also exhibited good agreement with Na^+%. Thus, from the irrigation suitability perspective, the overall water quality of the GRB water samples in all the monitoring periods lies under the safe category except for a few samples from the semi-arid segment of the upstream region.

4. Conclusion

This study explores and analyzes the geochemical characteristics of river water in the glacier-fed semi-arid and humid subtropical segments of the Gandaki River Basin in Nepal. It deals with the interactions of the river water with different spheres of the environment, such as hydrosphere, geosphere, atmosphere, anthroposphere and even cryosphere. The results reveal that most hydrochemical attributes exhibit significant spatiotemporal variations due to distinct lithology and monsoon driven-climatic seasonality, as well as complex interactions with anthropogenic components. The grand mean values of the major ions follow the order of $Ca^{2+} > Mg^{2+} > Na^+ > K^+$ for cations, and $HCO_3^- > SO_4^{2-} > Cl^- > NO_3^-$ for anions. The Piper plot implies that the prevailing water facies is the Ca-HCO_3 (>83%) type. Gibbs plot, principal component analysis and mixing diagram inferred that the primary mechanism controlling the hydrochemistry of the basin is rock weathering followed by

evapo-crystalization in the upstream segment. These findings were also confirmed by the relatively high ratios of $(Ca^{2+} + Mg^{2+}) / (Na^{+} + K^{+})$, $HCO_3^{-} / (Na^{+} + K^{+})$ and $(Ca^{2+} + Mg^{2+}) / Tz^{+}$.

The measured chemical attributes at a few locations pose safety concern for drinking and irrigation purposes compared to the WHO drinking water and irrigation water quality standards. The changing pattern of hydrogeochemistry, which is mainly controlled by climatic, geogenic and anthropogenic conditions, may have serious implications for the future water quality. The results emphasize the need for in-depth research in the lithologically and climatically complex Himalayan river basins to ensure the water quality and sustainability.

Acknowledgments

This research was financially supported by the International Partnership Program of Chinese Academy of Sciences (Grant No. 131C11KYSB20160061) and the National Natural Science Foundation of China (Grant No. 41422101).

Appendix A. Supplementary data

Supplementary data to this article can be found online at https://doi.org/10.1016/j.scitotenv.2017.12.063.

References

Ahmad, T., Khanna, P.P., Chakrapani, G.J., Balakrishnan, S., 1998. Geochemical characteristics of water and sediment of the Indus river, Trans-Himalaya, India: constraints on weathering and erosion. J. Asian Earth Sci. 16:333–346. https://doi.org/10.1016/S0743-9547(98)00016-6.

Amatya, K.M., Jnawali, B.M., 1994. Geological map of Nepal. Scale: 1: 1 000 000. Published by Department of Mines & Geology, Kathmandu, Nepal.

Apha, A., 2005. WEF, 2005. Stand. Methods Exam. Water Wastewater 21, 258–259.

Aryal, R.S., 2011. Water Resources of Nepal in the Context of Climate Change. Government of Nepal, Water and Energy Commission Secretariat.

Bajracharya, T.R., Acharya, S., Ale, B.B., 2011. Changing climatic parameters and its possible impacts in hydropower generation in Nepal (a case study on Gandaki River Basin). J. Inst. Eng. 8:160–173. https://doi.org/10.3126/jie.v8i1-2.5108.

Baral, U., Ding, L., Chamlagain, D., 2017. Detrital zircon ages and provenance of Neogene foreland basin sediments of the Karnali River section, Western Nepal Himalaya. J. Asian Earth Sci. 138:98–109. https://doi.org/10.1016/j.jseaes.2017.02.003.

Barnett, T.P., Adam, J.C., Lettenmaier, D.P., 2005. Potential impacts of a warming climate on water availability in snow-dominated regions. Nature 438:303–309. https://doi.org/10.1038/nature04141.

Bengraïne, K., Marhaba, T.F., 2003. Using principal component analysis to monitor spatial and temporal changes in water quality. J. Hazard. Mater. 100:179–195. https://doi.org/10.1016/S0304-3894(03)00104-3.

Bhatnagar, A., Devi, P., George, M.P., 2016. Impact of mass bathing and religious activities on water quality index of prominent water bodies: a multilocation study in Haryana, India. Int. J. Ecol. Environ. Sci. 2016. https://doi.org/10.1155/2016/2915905.

Bishara, A.J., Hittner, J.B., 2012. Testing the significance of a correlation with nonnormal data: comparison of Pearson, Spearman, transformation, and resampling approaches. Psychol. Methods 17:399–417. https://doi.org/10.1037/a0028087.

Chen, J., Wang, F., Xia, X., Zhang, L., 2002. Major element chemistry of the Changjiang (Yangtze River). Chem. Geol. 187, 231–255.

Dahal, P., Shrestha, N.S., Shrestha, M.L., Krakauer, N.Y., Panthi, J., Pradhanang, S.M., Jha, A., Lakhankar, T., 2016. Drought risk assessment in central Nepal: temporal and spatial analysis. Nat. Hazards 80:1913–1932. https://doi.org/10.1007/s11069-015-2055-5.

Dekov, V.M., Komy, Z., Van Put, A., Van Grieken, R., Araújo, F., Van Put, A., Van Grieken, R., 1997. Chemical composition of sediments, suspended matter, river water and ground water of the Nile (Aswan-Sohag traverse). Sci. Total Environ. 201:195–210. https://doi.org/10.1016/S0048-9697(97)84057-0.

Dhital, M.R., 2015. Geology of the Nepal Himalaya: Regional Perspective of the Classic Collided Orogen. Springer.

Diamantini, E., Lutz, S.R., Mallucci, S., Majone, B., Merz, R., Bellin, A., 2018. Driver detection of water quality trends in three large European river basins. Sci. Total Environ. 612: 49–62. https://doi.org/10.1016/j.scitotenv.2017.08.172.

Elango, L., 2005. Groundwater Quality and Its Suitability for Drinking and Agricultural Use in Chithar River Basin, Tamil Nadu, India. :pp. 1099–1110 https://doi.org/10.1007/s00254-005-1243-0.

English, N.B., Quade, J., DeCelles, P.G., Garzione, C.N., 2000. Geologic control of Sr and major element chemistry in Himalayan Rivers, Nepal. Geochim. Cosmochim. Acta 64, 2549–2566.

Fan, B.-L., Zhao, Z.-Q., Tao, F.-X., Liu, B.-J., Tao, Z.-H., Gao, S., Zhang, L.-H., 2014. Characteristics of carbonate, evaporite and silicate weathering in Huanghe River basin: a comparison among the upstream, midstream and downstream. J. Asian Earth Sci. 96, 17–26.

Flintrop, C., Hohlmann, B., Jasper, T., 1996. Anatomy of pollution: rivers of north Rhine-Westphalia, Germany. Am. J. Sci. 296.

Gaillardet, J., Dupré, B., Louvat, P., Allègre, C.J., 1999. Global silicate weathering and CO_2 consumption rates deduced from the chemistry of large rivers. Chem. Geol. 159: 3–30. https://doi.org/10.1016/S0009-2541(99)00031-5.

Galy, A., France-Lanord, C., 1999. Weathering processes in the Ganges–Brahmaputra basin and the riverine alkalinity budget. Chem. Geol. 159, 31–60.

Galy, A., France-Lanord, C., Derry, L.A., 1999. The strontium isotopic budget of Himalayan rivers in Nepal and Bangladesh. Geochim. Cosmochim. Acta 63, 1905–1925.

Gibbs, R.J., 1970. Mechanisms controlling world water chemistry. Science 170, 1088–1090.

Gotway, C.A., Helsel, D.R., Hirsch, R.M., 1994. Statistical methods in water resources. Technometrics 36:323. https://doi.org/10.2307/1269385.

Guo, Wang, F., Vogt, R.D., Zhang, Y., Liu, C.-Q., 2015. Anthropogenically enhanced chemical weathering and carbon evasion in the Yangtze Basin. Sci. Rep. 5:11941. https://doi.org/10.1038/srep11941.

Gustafsson, J.P., 2011. Visual MINTEQ Ver. 3.0. Dep. L. Water Resour. Eng. R. Inst. Technol, Stokholm, Sweden.

Haidary, A., Amiri, B.J., Adamowski, J., Fohrer, N., Nakane, K., 2013. Assessing the impacts of four land use types on the water quality of wetlands in Japan. Water Resour. Manag. 27:2217–2229. https://doi.org/10.1007/s11269-013-0284-5.

Hiroshi, S., Mikazu, Y., Randolph, C., 1999. Status of Geochemical Modeling of Groundwater Evolution at the Tono In-situ Tests Site, Japan. Japan Nuclear Cycle Development Institute.

Huang, X., Sillanpää, M., Duo, B., Gjessing, E., 2008. Water quality in the Tibetan Plateau: metal contents of four selected rivers. Environ. Pollut. 156.2, 270–277.

Huang, X., Sillanpää, M., Gjessing, E.T., Vogt, R.D., 2009. Water quality in the Tibetan Plateau: major ions and trace elements in the headwaters of four major Asian rivers. Sci. Total Environ. 407, 6242–6254.

Jiang, L., Yao, Z., Liu, Z., Wang, R., Wu, S., 2015. Hydrochemistry and its controlling factors of rivers in the source region of the Yangtze River on the Tibetan Plateau. J. Geochem. Explor. 155, 76–83.

Karim, A., Veizer, J., 2000. Weathering processes in the Indus River Basin: implications from riverine carbon, sulfur, oxygen, and strontium isotopes. Chem. Geol. 170, 153–177.

Khadka, U.R., Ramanathan, A.L., 2012. Major ion composition and seasonal variation in the Lesser Himalayan lake: case of Begnas Lake of the Pokhara Valley, Nepal. Arab. J. Geosci. 6:4191–4206. https://doi.org/10.1007/s12517-012-0677-4.

Le Fort, P., 1975. Himalayas: the collided range. Present knowledge of the continental arc. Am. J. Sci. 275, 44.

Lecomte, K.L., Pasquini, A.I., Depetris, P.J., 2005. Mineral weathering in a semiarid mountain river: its assessment through PHREEQC inverse modeling. Aquat. Geochem. 11, 173–194.

Lewis Jr., W.M., Hamilton, S.K., Jones, S.L., Runnels, D.D., 1987. Major element chemistry, weathering and element yields for the Caura River drainage, Venezuela. Biogeochemistry 4, 159–181.

Li, S., Gu, S., Tan, X., Zhang, Q., 2009a. Water quality in the upper Han River basin, China: the impacts of land use/land cover in riparian buffer zone. J. Hazard. Mater. 165: 317–324. https://doi.org/10.1016/j.jhazmat.2008.09.123.

Li, S., Xu, Z., Wang, H., Wang, J., Zhang, Q., 2009b. Geochemistry of the upper Han River basin, China: 3: anthropogenic inputs and chemical weathering to the dissolved load. Chem. Geol. 264, 89–95.

Lioubimtseva, E., Henebry, G.M., 2009. Climate and environmental change in arid Central Asia: impacts, vulnerability, and adaptations. J. Arid Environ. https://doi.org/10.1016/j.jaridenv.2009.04.022.

López-Moreno, J.I., Vicente-Serrano, S.M., Moran-Tejeda, E., Zabalza, J., Lorenzo-Lacruz, J., García-Ruiz, J.M., 2011. Impact of climate evolution and land use changes on water yield in the Ebro basin. Hydrol. Earth Syst. Sci. 15, 311.

Manandhar, S., Pandey, V.P., Kazama, F., 2012. Application of Water Poverty Index (WPI) in Nepalese context: a case study of Kali Gandaki River Basin (KGRB). Water Resour. Manag. 26:89–107. https://doi.org/10.1007/s11269-011-9907-x.

Meybeck, M., 1987. Global chemical weathering of surficial rocks estimated from river dissolved loads. Am. J. Sci. 287, 401–428.

Meybeck, M., 2003. Global occurrence of major elements in rivers. Treatise on Geochemistry. 5, pp. 207–223.

Mishra, B., Babel, M.S., Tripathi, N.K., 2014. Analysis of climatic variability and snow cover in the Kaligandaki River Basin, Himalaya, Nepal. Theor. Appl. Climatol. 116:681–694. https://doi.org/10.1007/s00704-013-0966-1.

MOAD, N., 2012. Statistical Information on Nepalese Agriculture Government of Nepal Ministry of Agricultural Development Agri-Business Promotion and Statistics Division Agristatistics Section.

Moon, S., Huh, Y., Zaitsev, A., 2009. Hydrochemistry of the Amur river: weathering in a northern temperate basin. Aquat. Geochem. 15, 497–527.

Mortatti, J., Probst, J.-L., 2003. Silicate rock weathering and atmospheric/soil CO_2 uptake in the Amazon basin estimated from river water geochemistry: seasonal and spatial variations. Chem. Geol. 197, 177–196.

Neupane, B., Ju, Y., Allen, C.M., Ulak, P.D., Han, K., 2017. Petrography and provenance of Upper Cretaceous – Palaeogene sandstones in the foreland basin system of Central Nepal. Int. Geol. Rev. 0:1–22. https://doi.org/10.1080/00206814.2017.1312716.

Pacheco Castro, R., Pacheco Ávila, J., Ye, M., Cabrera Sansores, A., 2017. Groundwater quality: analysis of its temporal and spatial variability in a karst aquifer. Groundwater: 1–11 https://doi.org/10.1111/gwat.12546.

Panthi, J., Dahal, P., Shrestha, M.L., Aryal, S., Krakauer, N.Y., Pradhanang, S.M., Lakhankar, T., Jha, A.K., Sharma, M., Karki, R., 2015. Spatial and temporal variability of rainfall in the Gandaki River Basin of Nepal Himalaya. Climate 3, 210–226.

Paudel, K.P., Andersen, P., 2011. Monitoring snow cover variability in an agropastoral area in the Trans Himalayan region of Nepal using MODIS data with improved cloud removal methodology. Remote Sens. Environ. 115, 1234–1246.
Paudyal, R., Kang, S., Sharma, C.M., Tripathee, L., Huang, J., Rupakheti, D., Sillanpää, M., 2016a. Major ions and trace elements of two selected rivers near Everest region, southern Himalayas, Nepal. Environ. Earth Sci. 75, 1–11.
Paudyal, R., Kang, S., Sharma, C.M., Tripathee, L., Sillanpää, M., 2016b. Variations of the Physicochemical Parameters and Metal Levels and Their Risk Assessment in Urbanized Bagmati River, Kathmandu, Nepal. https://doi.org/10.1155/2016/6025905.
Peter, J., Anandhan, P., 2008. Identification of Major Sources Controlling Groundwater Chemistry From a Hard Rock Terrain – A Case Study From Mettur taluk, Salem District, Tamil Nadu, India. pp. 49–58.
Piper, A.M., 1944. A graphic procedure in the geochemical interpretation of water-analyses. EOS Trans. Am. Geophys. Union 25, 914–928.
Quade, J., English, N., DeCelles, P.G., 2003. Silicate versus carbonate weathering in the Himalaya: a comparison of the Arun and Seti River watersheds. Chem. Geol. 202, 275–296.
Ramanathan, A.L., 2007. Seasonal variation in the major ion chemistry of Pandoh Lake, Mandi district, Himachal Pradesh, India. Appl. Geochem. 22, 1736–1747.
Richards, L.A., 1954. Diagnosis and Improvement of Saline and Alkali Soils. LWW.
Saleh, A., Shehata, M., 1999. Hydrogeochemical Processes Operating within the Main Aquifers of Kuwait. pp. 195–209.
Sarin, M.M., Krishnaswami, S., Dilli, K., Somayajulu, B.L.K., Moore, W.S., 1989. Major ion chemistry of the Ganga-Brahmaputra river system: weathering processes and fluxes to the Bay of Bengal. Geochim. Cosmochim. Acta 53, 997–1009.
Şener, Ş., Şener, E., Davraz, A., 2017. Evaluation of water quality using water quality index (WQI) method and GIS in Aksu River (SW-Turkey). Sci. Total Environ. 584–585: 131–144. https://doi.org/10.1016/j.scitotenv.2017.01.102.
Sharif, M.U., Davis, R.K., Steele, K.F., Kim, B., Kresse, T.M., Fazio, J.A., 2008. Inverse geochemical modeling of groundwater evolution with emphasis on arsenic in the Mississippi River valley alluvial aquifer, Arkansas (USA). J. Hydrol. 350, 41–55.
Sharma, A., Singh, A.K., Kumar, K., 2012. Environmental geochemistry and quality assessment of surface and subsurface water of Mahi River basin, western India. Environ. Earth Sci. 65, 1231–1250.
Singh, P.K., Malik, A., Mohan, D., Sinha, S., 2004. Multivariate statistical techniques for the evaluation of spatial and temporal variations in water quality of Gomti River (India)—a case study. Water Res. 38, 3980–3992.
Singh, V.B., Ramanathan, A.L., Pottakkal, J.G., Kumar, M., 2014. Seasonal variation of the solute and suspended sediment load in Gangotri glacier meltwater, central Himalaya, India. J. Asian Earth Sci. 79, 224–234.
Singh, V.B., Ramanathan, A.L., Mandal, A., 2016. Hydrogeochemistry of high-altitude lake: a case study of the Chandra Tal, Western Himalaya, India. Arab. J. Geosci. 9, 1–9.
Stallard, R.F., Edmond, J.M., 1983. Geochemistry of the Amazon: 2. The influence of geology and weathering environment on the dissolved load. J. Geophys. Res. Oceans 88, 9671–9688.
Stallard, R.F., Edmond, J.M., 1987. Geochemistry of the Amazon: 3. Weathering chemistry and limits to dissolved inputs. J. Geophys. Res. Oceans 92, 8293–8302.
Sun, H., Han, J., Li, D., Zhang, S., Lu, X., 2010. Chemical weathering inferred from riverine water chemistry in the lower Xijiang basin, South China. Sci. Total Environ. 408, 4749–4760.
Thomas, J., Joseph, S., Arunkumar, T.M.M.K.S., 2014. Seasonal Variation in Major Ion Chemistry of a Tropical Mountain River, the Southern Western Ghats, Kerala, India. :pp. 2333–2351 https://doi.org/10.1007/s12665-013-2634-2.
Thomas, J., Joseph, S., Thrivikramji, K.P., 2015. Hydrochemical variations of a tropical mountain river system in a rain shadow region of the southern Western Ghats, Kerala, India. Appl. Geochemistry 63, 456–471.
Tripathee, L., Kang, S., Huang, J., Sillanpää, M., Sharma, C.M., Lüthi, Z.L., Guo, J., Paudyal, R., 2014. Ionic composition of wet precipitation over the southern slope of central Himalayas, Nepal. Environ. Sci. Pollut. Res. 21, 2677–2687.
Tripathee, L., Kang, S., Sharma, C.M., 2016. Preliminary Health Risk Assessment of Potentially Toxic Metals in Surface Water of the Himalayan Rivers, Nepal. 97:pp. 855–862. https://doi.org/10.1007/s00128-016-1945-x.
Trower, L., 2009. Spatial variations in chemical weathering and CO_2 consumption in Nepalese High Himalayan catchments during the monsoon season. Geochim. Cosmochim. Acta https://doi.org/10.1016/j.gca.2009.06.036.
Turchyn, A.V., Tipper, E.T., Galy, A., Lo, J.K., Bickle, M.J., 2013. Isotope evidence for secondary sulfide precipitation along the Marsyandi River, Nepal, Himalayas. Earth Planet. Sci. Lett. 374, 36–46.
Uddin, K., Shrestha, H.L., Murthy, M.S.R., Bajracharya, B., Shrestha, B., Gilani, H., Pradhan, S., Dangol, B., 2015. Development of 2010 national land cover database for the Nepal. J. Environ. Manag. 148:82–90. https://doi.org/10.1016/j.jenvman.2014.07.047.
Upreti, B.N., 1999. An overview of the stratigraphy and tectonics of the Nepal Himalaya. J. Asian Earth Sci. 17, 577–606.
Varol, M., Gökot, B., Bekleyen, A., Şen, B., 2013. Geochemistry of the Tigris River basin, Turkey: spatial and seasonal variations of major ion compositions and their controlling factors. Quat. Int. 304, 22–32.
Vrebos, D., Beauchard, O., Meire, P., 2017. The impact of land use and spatial mediated processes on the water quality in a river system. Sci. Total Environ. 601–602: 365–373. https://doi.org/10.1016/j.scitotenv.2017.05.217.
Wang, G., Wang, Y., Li, Y., Cheng, H., 2007. Influences of alpine ecosystem responses to climatic change on soil properties on the Qinghai–Tibet Plateau, China. Catena 70, 506–514.
WHO, 2011. Guidelines for drinking-water quality. WHO Chronicle. World Health Organization, Geneva.
Wilcox, L.V., 1948. The Quality of Water for Irrigation Use. United States Department of Agriculture, Economic Research Service.
Xiao, J., Jin, Z.-D., Ding, H., Wang, J., Zhang, F., 2012. Geochemistry and solute sources of surface waters of the Tarim River Basin in the extreme arid region, NW Tibetan Plateau. J. Asian Earth Sci. 54, 162–173.
Xiao, J., Jin, Z.D., Wang, J., Zhang, F., 2015. Hydrochemical characteristics, controlling factors and solute sources of groundwater within the Tarim River Basin in the extreme arid region, NW Tibetan Plateau. Quat. Int. 380–381:237–246. https://doi.org/10.1016/j.quaint.2015.01.021.
Yao, T., Thompson, L., Yang, W., Yu, W., Gao, Y., Guo, X., Yang, X., Duan, K., Zhao, H., Xu, B., 2012. Different glacier status with atmospheric circulations in Tibetan Plateau and surroundings. Nat. Clim. Chang. 2, 663–667.
Zhang, J., Huang, W.W., Letolle, R., Jusserand, C., 1995. Major element chemistry of the Huanghe (Yellow River), China-weathering processes and chemical fluxes. J. Hydrol. 168, 173–203.
Zhang, F., Yeh, G.-T., Parker, J.C., Zhang, H., Shi, X., Wang, C., Gu, R., 2012. A reaction-based river/stream water quality model: reaction network decomposition and model application. Terr. Atmos. Ocean. Sci. 23.